ELSEVIER

Applied Ocean Research 20 (1998) 145–156

Applied Ocean Research

Current forces in tankers and bifurcation of equilibrium of turret systems: hydrodynamic model and experiments

A.J.P. Leite[a], J.A.P. Aranha[b], C. Umeda[c], M.B. de Conti[b]

[a]*E&P, Petrobrás, Rio de Janeiro, Brazil*
[b]*Department of Naval Engineering, EPUSP, San Paulo, Brazil*
[c]*Department of Naval Engineering, IPT, San Paulo, Brazil*

Received for publication 27 January 1998

Abstract

In the present paper a heuristic hydrodynamic model is proposed to describe the forces and moment in the horizontal plane in a tanker caused by an ocean current. The obtained expressions depend only on the incidence angle of the current, on the main dimensions of the ship and on some well known hydrodynamic coefficients. The results from this model were confronted with experimental values obtained by Wichers (*A Simulation Model for a Single Point Moored Tanker*, Publ. 797, MARIN, Wageningen, the Netherlands, 1988) and at IPT's test basin, the observed adherence being reasonably good for all current headings. A special device was used to experimentally study the stability of the equilibrium of a tanker free to rotate around a vertical axis and with the other's movements constrained, emulating a turret system with stiff mooring lines. In this situation the only bifurcation parameter is the turret position, and the proposed hydrodynamic model was able to predict, with reasonable accuracy, the critical value of this parameter. Furthermore, the adherence between the experimental and theoretical models in the post-critical region was very consistent, disclosing that the post-critical behavior is dominated by the parcel $C_Y\Psi|\Psi|$, where C_Y is the lateral force coefficient in beam current and Ψ is the angle between the current and the ship's longitudinal axis. It turns out that, in the vicinity of the bifurcation point, the yaw angle increases linearly with the bifurcation parameter and not with its square root, as a standard approach would suggest, based on Taylor's series expansion (hydrodynamic derivatives).

1. Introduction

The oil industry has become interested lately in studying the technical feasibility of large tankers as floating production systems in deep water. To minimize the requirements on the mooring lines it is certainly desirable to weathervane the ship, allowing an automatic alignment of its axis with the resultant of the environmental loads. One of the possible alternatives in this context is to introduce a turret, namely, an articulation around which the ship can rotate freely until its axis is coincident with the direction of the resultant forces.

Technical aspects of the turret system have been discussed in the literature recently[1,2], while the intricate dynamic behavior of both a single point or spread mooring systems has been subjected to intense study by the academic community[3–8]. These studies use the maneuvering equations of motion, with hydrodynamics derivatives obtained, in general, from Obokata *et al.*[9] or Takashina[10], and address the problem either from a qualitative dynamic approach or else from a direct time domain simulation.

As an outcome of this study a variety of dynamic behaviors has been disclosed, including bifurcation of equilibrium, limit cycles and chaotic response, the boundaries defining the transition from one type of response to another depending both on the order of the maneuvering equation chosen and the hydrodynamic coefficients used. Obviously, questions about the *structural stability* of the model and its *robustness* with respect to variations of the hydrodynamic coefficients naturally arise and should not be overlooked if the intention is to use these models as a design tool. Besides, the experimental confirmation of most results is still weak and sometimes blurred by the fact that it is difficult to interpret an experimental result when too many variables are involved.

Motivated by this observation, the intention of this work is to present and discuss experimental results obtained in a simplified configuration, by restricting the degrees of freedom and, as a consequence, the variability of possible dynamic behaviors. More specifically, the devised experiment consisted to pull the model with uniform velocity while allowing it to have only one degree of freedom, namely, the freedom to rotate around an articulation (turret) placed at a given distance from the midship section. By changing the position of the articulation one could not only determine experimentally its *critical position* (bifurcation point) but also the *post-critical behavior* of the system

0141-1187/98/$19.00
PII S0141-1187(98)00002-9

as a function of the bifurcation parameter, given by the distance between the critical and the actual position of the articulation.

With this simplified physical model one loses the rich dynamic pattern discussed in the literature, but, on the other hand, a very clear picture of the (static) bifurcation phenomenon is obtained. In particular, one could show that the yaw angle Ψ, which defines the stable equilibrium position in the post-critical region, increases linearly with the bifurcation parameter, and not with its square root, as a standard Taylor's series expansion approach (hydrodynamic derivatives) would suggest. This result is caused by the fact that the dominating nonlinear term is of the form $C_Y\Psi|\Psi|$, with C_Y being the lateral force coefficient in beam current. It turns out then that static bifurcation phenomenon can be predicted with some accuracy, since the experimental determination of the lateral force coefficient C_Y is relatively precise, due to the magnitude of this force; furthermore, the present analysis suggests that the influence of this term cannot be ignored in the more complex dynamic study, such as those quoted above.

In Section 2 of this work a simple, heuristic, hydrodynamic model is proposed to describe the generalized current forces in a tanker as a function of the incidence angle of the current, of the main ship's dimension and some few hydrodynamic coefficients; in Section 3 the stability of the equilibrium of a tanker, with its only degree of freedom being the rotation around the turret, is analyzed. In Section 4 the experimental results are presented, showing both the accuracy of the hydrodynamic model for an arbitrary incidence angle and its adequacy for the study of the bifurcation phenomenon under consideration.

2. Hydrodynamic model

One considers here a coordinate system with origin at the midship section, the z-axis being vertical and pointing upwards, the x-axis being in the longitudinal direction, from stern to bow, and the y-axis positive to portside. The ocean current is supposed to have velocity U and is incident in a direction that makes an angle α with the x-axis; the velocity vector $\mathbf{U}$ is then given by:

$$\mathbf{U} = U\cdot[\cos\alpha i + \sin\alpha j] \tag{1}$$

Let $X_C(\alpha)$ be the longitudinal force, $Y_C(\alpha)$ the lateral force and $N_C(\alpha)$ the yaw moment, with the resultant assumed to be applied at the midship section. Following Wichers[11], the forces will be normalized by the ship's draft T and ship's length L, in such way that:

$$X_C(\alpha) = \tfrac{1}{2}\rho TL\cdot C_{1C}(\alpha)\cdot U^2, \tag{2}$$

$$Y_C(\alpha) = \tfrac{1}{2}\rho TL\cdot C_{2C}(\alpha)\cdot U^2,$$

$$N_C(\alpha) = \tfrac{1}{2}\rho TL^2\cdot C_{6C}(\alpha)\cdot U^2$$

The intention now is to use some heuristic hydrodynamic model to express the functions $\{C_{1C}(\alpha); C_{2C}(\alpha); C_{6C}(\alpha)\}$ in terms of well defined hydrodynamic coefficients and of the ship's main dimensions, namely: the length L, the beam B, the draft T, the block coefficient C_B and the wetted surface S.

In the computation of the forces $\{X_C(\alpha); Y_C(\alpha)\}$ it will be assumed below, for the sake of simplicity, that the ship is symmetric with respect to the midsection, although the actual non-symmetry of the ship is considered in the estimation of the yaw moment $N_C(\alpha)$.

For a current in the longitudinal direction ($\alpha = 0°$; $\alpha = 180°$) two hydrodynamic coefficients are important: the *skin friction* coefficient $C_F(R_e)$ and the *factor of form* k. Taking the ITTC friction line for $C_F(R_e)$ and the Prohaska method, assuming nearly zero Froude number, to estimate k, one obtains[12].

$$C_{1C}(0°) = C_{1C}(180°) = (1+k)\cdot\frac{0.075}{(\log_{10}R_e - 2)^2}\cdot\frac{S}{TL}; \tag{3a}$$

$$k = 0.25$$

One certainly should expect a small difference in $C_{1C}(\alpha)$ when $\alpha = 0°$ and $\alpha = 180°$, but this difference is ignored in the proposed model. For a current in the beam direction ($\alpha = 90°$; $\alpha = 270°$) the lateral force coefficient is related to the *two-dimensional* cross-flow coefficient C_D, function of the ratio $B/2T$ and of the bilge radius[13]. Observing that three-dimensional effects should decrease the value of the cross-flow coefficient, one can either correct the two-dimensional value, introducing a 'slenderness parameter', or else, as a first estimate, to take the lower bound of the two-dimensional coefficients given in Hoerner, corresponding to the greatest bilge radius ($r_C/2T \cong 0.5$); just for reference this curve is presented at Fig. 1.

Naming by C_Y the cross-flow coefficient for the actual ship, one has

$$C_{2C}(90°) = -C_{2C}(270°) = C_Y \tag{3b}$$

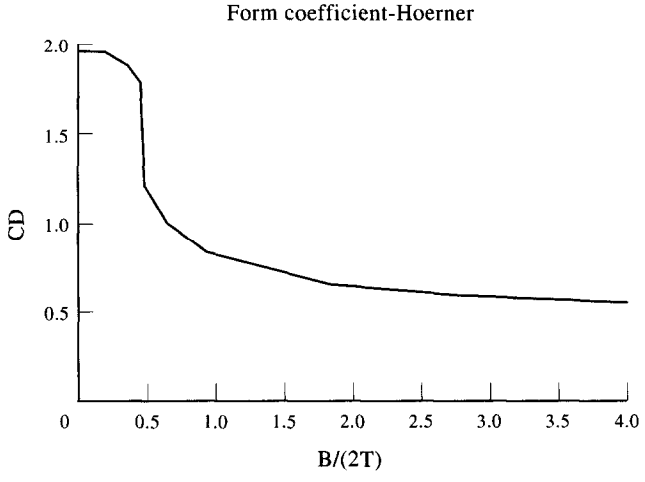

Fig. 1. Two-dimensional cross-flow coefficient C_D as a function of $B/2T$[13].

where one can use Hoerner's curve as a first estimate for ($C_Y \cong C_D(B/2T)$).

If the ship were strictly symmetric with respect to the y-axis no yaw moment could be detected for a current incident in the beam direction. The lack of symmetry implies that a small moment must exist, since then the resultant of the lateral force should pass by a point distant l from the midsection, in general aft of this section, leading to an expression of the form

$$C_{6C}(90°) = -C_{6C}(270°) = -\frac{l}{L}C_Y \tag{3c}$$

As it will be seen in Section 4, the value of l/L is small, although the relative variability is large: it ranges from roughly 1% to 8% for the different ships analyzed both by Wichers[11] and at the IPT's test basin; as a first guess one may take $l/L \approx 5\%$.

Once introduced the hydrodynamic coefficients $\{(1+k)C_F(R_e);\ C_Y;\ l/L\}$, the force coefficients $\{C_{1C}(\alpha);\ C_{2C}(\alpha);\ C_{6C}(\alpha)\}$ can be inferred from some simple arguments, as discussed below.

2.1. The longitudinal force coefficient $C_{1C}(\alpha)$

The function $C_{1C}(\alpha)$ is periodic in α and can be expanded in Fourier series. From the symmetry with respect to the x-axis one has $C_{1C}(\alpha) = C_{1C}(-\alpha)$ and so only terms of the form $\cos(n\alpha)$ can appear in this series; assuming also the symmetry with respect to the y-axis one should have $C_{1C}(\alpha) = -C_{1C}(\pi - \alpha)$ and so only the odd terms $\cos[(2n+1)\alpha]$ can be present. Taking only two terms in the series the following approximation is proposed:

$$\frac{C_{1C}(\alpha)}{C_{1C}(0°)} \cong a_1\cos\alpha + a_3\cos 3\alpha; \tag{4a}$$

$$a_1 + a_3 = 1$$

The intention now is to use known results for a wing of low aspect ratio to obtain convenient expressions for the Fourier coefficients $\{a_1; a_2\}$. For a *flat plate* with aspect ratio $A = 2T/L \ll 1$ the lift coefficient C_L and induced drag coefficient C_D are given by the relations ($\alpha \ll 1$):

$$C_L = \frac{\pi A}{2}\sin\alpha;\ C_D = \frac{C_L^2}{\pi A} \tag{4b}$$

Projecting the total drag and lift forces in the longitudinal direction one obtains, for a *flat plate*, that

$$C_{1C}(\alpha) \cong \left[C_F(R_e) + C_D\right]\cos\alpha - C_L\sin\alpha \tag{4c}$$

Observing that $C_{1C}(0°) = C_F(R_e)$ in this case and expanding the above expression, together with Eq. (4a), in power series in α up to the order α^2, the following relations can be derived:

$$a_1 = 1 - \frac{1}{C_F(R_e)}\cdot\frac{\pi T}{8L};$$

$$a_3 = \frac{1}{C_F(R_e)}\cdot\frac{\pi T}{8L}$$

It turns out then that, for a *flat plate*, the longitudinal force coefficient can be approximated by

$$C_{1C}(\alpha) \cong C_F(R_e)\cos\alpha + \frac{1}{8}\frac{\pi T}{L}(\cos 3\alpha - \cos\alpha)$$

A similar expression is now proposed for the ship, the only modification being to change the flat plate resistance coefficient $C_F(R_e)$ by the ship's resistance coefficient (Eq. (4a)); the final result is

$$C_{1C}(\alpha) \cong \left(\frac{0.09375}{(\log_{10}R_e - 2)^2}\cdot\frac{S}{TL}\right)\cdot\cos\alpha + \frac{1}{8}\frac{\pi T}{L}(\cos 3\alpha - \cos\alpha) \tag{5}$$

The only point that deserves attention here is to observe that the Fourier series Eq. (4a) gives a rationality to spread, for all values of α, results that were thought to be valid only for small α (wing theory). In this context, one could have used directly Eq. (4b) and Eq. (4c), an alternative that will be explored in the next item.

2.2. The lateral force coefficient $C_{2C}(\alpha)$

For $|\sin\alpha|0(1)$ the basic mechanism that determines the lateral force is the cross-flow, identified with the hydrodynamic coefficient C_Y; if the body is slender one may take $C_Y \sin\alpha|\sin\alpha|$ as the related force coefficient[14]. One should add now the lift and induced drag forces obtained from the low aspect wing theory (see Eq. (4b)) but, in doing so, the actual cross-flow coefficient must be corrected in order to maintain Eq. (3b); the following expression is then proposed for the lateral force coefficient:

$$C_{2C}(\alpha) \cong \left(C_Y - \frac{\pi T}{2L}\right)\sin\alpha|\sin\alpha| + \frac{\pi T}{2L}\sin^3\alpha + \frac{\pi T}{L}\sin\alpha|\cos\alpha| \tag{6a}$$

The behavior of $C_{2C}(\alpha)$ for small α is essential in the stability analysis, although, in the above expression, this term is dominated by the *flat plate* result $(\pi T/L)\alpha$. One should expect that the stability performance of the ship is influenced by some *form coefficient* and, in fact, after an extensive statistical analysis of several ship maneuvering experiments Clarke *et al.*[15] suggested the following *linear* hydrodynamic derivative:

$$C_{2C}(\alpha) \cong \frac{\pi T}{L}\left(1 + 0.4\frac{C_B B}{T}\right)\cdot\alpha;\ \alpha < 1 \tag{6b}$$

Incorporating Eq. (6b) into Eq. (6a), the force coefficient $C_{2C}(\alpha)$ can finally be approximated by the expression:

$$C_{2C}(\alpha) \cong \left(C_Y - \frac{\pi T}{2L}\right)\sin\alpha|\sin\alpha| + \frac{\pi T}{2L}\sin^3\alpha + \frac{\pi T}{L}\left(1 + 0.4\frac{C_B B}{T}\right)\sin\alpha|\cos\alpha| \tag{7}$$

The first parcel in Eq. (7) can be interpreted as the two-dimensional cross-flow coefficient attenuated by the 'slenderness parameter' $\pi T/2L$, the second parcel is related to the induced drag of the low aspect ratio wing and the last one to the lift force in this surface.

2.3. The yaw moment coefficient $C_{6C}(\alpha)$

When $|\sin\alpha| \cong 0(1)$ the lateral force is dominated by the cross-flow component, passing in a point distant l from the origin; adding to the moment of this force the Munk's moment one has:

$$C_{6C}(\alpha) \cong -\frac{l}{L}\left(C_Y - \frac{\pi T}{2L}\right)\sin\alpha|\sin\alpha| - \frac{\pi T}{L}\sin\alpha\cos\alpha;\ |\sin\alpha| \cong 0(1) \tag{8a}$$

For $\alpha \approx \pi$ the lateral force is basically given by the lift on the low aspect ratio wing and, as it is known, in a rectangular wing this force is applied at the leading edge, giving rise to a moment that is half the Munk's moment value indicated in Eq. (8a). Observing this result, and also that this moment should depend on some *form coefficient*, after analyzing several experimental results Clarke *et al.*[15] suggested the expression

$$C_{6C}(\alpha) \cong \frac{\pi T}{L}\left(\frac{1}{2} + 2.4\frac{T}{L}\right)\sin\alpha;\ \alpha \approx \pi \tag{8b}$$

Observing that some *form factor* should be incorporated to the Munk's moment Eq. (8a), one can join Eq. (8a) and Eq. (8b) using a 'transition function', as e.g. $(1 + |\cos\alpha|/2)^2$, to obtain

$$C_{6C}(\alpha) \cong -\frac{l}{L}\left(C_Y - \frac{\pi T}{2L}\right)\sin\alpha|\sin\alpha| - \frac{\pi T}{L}\sin\alpha\cos\alpha - \left(\frac{1+|\cos\alpha|}{2}\right)^2 \frac{\pi T}{L}\left(\frac{1}{2} - 2.4\frac{T}{L}\right)\sin\alpha|\cos\alpha| \tag{9}$$

The last parcel in Eq. (9) corrects the flat plate Munk's moment $(\pi T/L)\sin\alpha\cos\alpha$ in a non-symmetric way: it decreases this value when $\alpha \approx \pi$ while increasing it when $\alpha \approx 0$. This result is consistent with the fact that the effect of the rudder as a stabilizing (destabilizing) fin when $\alpha \approx \pi$ ($\alpha \approx 0$) it is implicitly assumed here. If one intends to consider the bare hull moment the effect of the rudder has to be subtracted from Eq. (9) in the way indicated in Clarke *et al.*[15].

In Section 4 the Eqs. (5), (7) and (9) will be compared with the experimental results described in Wichers[11] and with experiments done at IPT's test basin.

3. Stability and bifurcation analysis

One can imagine here that the tanker has an articulation (turret), placed at a distance aL from the midsection, and

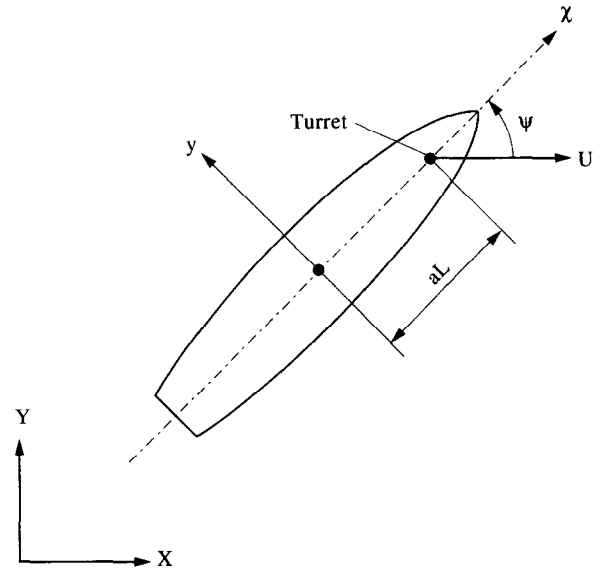

Fig. 2. Sketch of the model in the bifurcation experiment.

that a vertical bar, passing through the articulation, is being towed with a velocity U in the spatial X-direction, supposed to coincide initially with the longitudinal direction of the ship (see Fig. 2). In this set up the only degree of freedom left for the tanker is the yaw displacement Ψ, which measures the angle between the ship's longitudinal axis and the pulling direction X. In the reference system moving with the ship one sees a current with intensity U incident in the direction

$$\alpha = \pi - \Psi \tag{10a}$$

One can define here the non-dimensional *restoring* moment $N(\Psi)$ by the expression

$$\frac{\pi T}{L}\left(1 + 0.40\frac{C_B B}{T}\right)\cdot N(\Psi) = -\frac{Y_C(\alpha)\cdot aL - N_C(\alpha)}{\frac{1}{2}\rho T L^2 U^2}$$

the term in the left hand side being introduced by commodity; using Eq. (2) in this equality one obtains:

$$N(\Psi) = -\frac{L}{\pi T}\frac{1}{1 + 0.40C_B B/T}\left(C_{2C}(\alpha)\cdot a - C_{6C}(\alpha)\right) \tag{10b}$$

Placing Eq. (10a) into Eqs. (7) and (9), expanding these functions in power series of Ψ and retaining only terms to the order Ψ^3, the following expressions can be derived:

$$C_{2C}(\alpha) = \left(C_Y - \frac{\pi T}{2L}\right)\Psi|\Psi| + \frac{\pi T}{2L}\Psi^3 + \frac{\pi T}{L}\left(1 + 0.40\frac{C_B B}{T}\right)\cdot\left(\Psi - \frac{2}{3}\Psi^3\right); \tag{10c}$$

$$C_{6C}(\alpha) = -\frac{l}{L}\left(C_Y - \frac{\pi T}{2L}\right)\Psi|\Psi| + \frac{\pi T}{2L}\left(\frac{1}{2} - 2.4\frac{T}{L}\right)\Psi^3 + \frac{\pi T}{L}\left(\frac{1}{2} + 2.4\frac{T}{L}\right)\cdot\left(\Psi - \frac{2}{3}\Psi^3\right)$$

Introducing the parameter

$$a_{CR} = \frac{\frac{1}{2} + 2.4\frac{T}{L}}{1 + 0.40\frac{C_B B}{T}} \tag{11}$$

the *restoring* moment $N(\Psi)$ can be written as

$$-N(\Psi) = A(a)\cdot\Psi^3 + B(a)\cdot\Psi|\Psi| - C(a)\cdot\Psi \tag{12a}$$

with:

$$A(a) = \frac{2}{3}(a_{CR} - a) + \frac{\frac{a}{2} - \frac{1}{4} + 1.2\frac{T}{L}}{1 + 0.40\frac{C_B B}{T}}; \tag{12b}$$

$$B(a) = \left(\frac{LC_Y}{\pi T} - \frac{1}{2}\right)\cdot\frac{a + l/L}{1 + 0.40\frac{C_B B}{T}};$$

$$C(a) = (a_{CR} - a)$$

Observing that $l > 0$ and $0 \le a \le 0.5$, since the turret is usually placed ahead the midship section, then, necessarily, $B(a) > 0$. The sign of $C(a)$ changes from negative to positive as a decreases while the sign of $A(a)$ may or may not change with a, depending on the ship's main dimensions.

3.1. Equilibrium and stability conditions

If Ψ_e is such that $N(\Psi_e) = 0$ then, in theory at least, the ship can be pulled in the X-direction with velocity U while maintaining a constant yaw angle Ψ_e; this angle defines an *equilibrium configuration* of the system. In reality, this equilibrium configuration will be actually observed if and only if it is *stable*, namely: if a small perturbation $\delta\Psi$ on Ψ_e introduces a moment that tends to restore the original equilibrium configuration. Using the Taylor's series expansion

$$N(\Psi_e + \delta\Psi) = N(\Psi_e) + \left(\frac{\partial N}{\partial \Psi}\right)_{\Psi_e}\cdot\delta\Psi + (\ldots)$$

and recalling that $N(\Psi_e) = 0$, the moment $N(\Psi_e + \delta\Psi)$ will be *restoring* if and only if it has the opposite sign of $\delta\Psi$. The following conditions define then a *stable equilibrium configuration*:

$$N(\Psi_e) = 0 \text{ (equilibrium)}; \tag{13a}$$

$$\left(\frac{\partial N}{\partial \Psi}\right)_{\Psi_e} < 0 \text{ (stability)}$$

In terms of the cubic 'polynomial' (Eq. (12a)) these conditions can be written in the form:

$$A(a)\Psi_e^3 + B(a)\Psi_e|\Psi_e| - C(a)\Psi_e = 0 \text{ (equilibrium)}; \tag{13b}$$

$$3A(a)\Psi_e^2 + 2B(a)|\Psi_e| - C(a) > 0 \text{ (stability)}$$

The *trivial equilibrium position* $\Psi_e = 0$ will then be *stable* if and only if $a > a_{CR}(C(a) < 0)$, where $a_{CR}L$ is defined as the *critical position* of the turret. For $\Psi_e \neq 0$ the equilibrium equation reduces to the form

$$A(a)\Psi_e^2 + B(a)|\Psi_e| - C(a) = 0 \tag{14a}$$

while the *stability criteria* can be written as

$$-B(a)|\Psi_e| + 2C(a) > 0;\ \Psi_e \neq 0 \tag{14b}$$

or else in the form

$$2A(a)\Psi_e^2 + B(a)|\Psi_e| > 0;\ \Psi_e \neq 0 \tag{14c}$$

Observing that $B(a) > 0$, the only stable equilibrium position when $a > a_{CR}$ is the trivial solution $\Psi_e = 0$, since the stability criteria (Eq. (14b)), valid for $\Psi_e \neq 0$, cannot be satisfied when $a > a_{CR}(C(a) < 0)$. The post-critical behavior, when $a < a_{CR}$, will be analyzed next.

3.2. Bifurcation and post-critical behavior

When $a < a_{CR}(C(a) > 0)$ the roots of Eq. (14a) depend on the sign of $A(a)$. For $A(a) > 0$ the only possible roots are

$$\Psi_e = \pm\left\{-\frac{B(a)}{2A(a)} + \sqrt{\left(\frac{B(a)}{2A(a)}\right)^2 + \frac{C(a)}{A(a)}}\right\};\ A(a) > 0 \tag{15a}$$

From Eq. (14c) it follows, at once, that these equilibrium positions are stable ($A(a) > 0$). If $A(a) < 0$ the roots of Eq. (14a) are given by

$$\Psi_e = \pm\left\{\frac{B(a)}{2|A(a)|} \pm \sqrt{\left(\frac{B(a)}{2A(a)}\right)^2 - \frac{C(a)}{|A(a)|}}\right\};\ A(a) < 0$$

and the stability criteria (Eq. (14c)) can be rewritten in the form:

$$-2|A(a)|\cdot|\Psi_e|\left(|\Psi_e| - \frac{B(a)}{2|A(a)|}\right) > 0$$

It turns out that the only stable roots are given by:

$$\Psi_e = \pm\left\{\frac{B(a)}{2|A(a)|} - \sqrt{\left(\frac{B(a)}{2A(a)}\right)^2 - \frac{C(a)}{|A(a)|}}\right\};\ A(a) < 0 \tag{15b}$$

For $0 \le a_{CR} - a \ll 1 (0 \le C(a) \ll 1)$ both Eq. (15a) and Eq. (15b) can be approximated by

$$\Psi_e = \pm\frac{a_{CR} - a}{B(a)};\ 0 \le a_{CR} - a < 1 \tag{15c}$$

showing that the *stable equilibrium angle* increases *linearly* with the *bifurcation parameter* $a_{CR} - a$ in the vicinity of the bifurcation point. This result must be contrasted with the result obtained from the standard Taylor's series expansion method (hydrodynamic derivatives) where, in general, the parcel $B(a)\Psi_e|\Psi_e|$ is overlooked; in this case one can check easily (take $B(a) = 0$ in Eq. (15a)) that the stable equilibrium angle increases with the *square root* of the bifurcation

Table 1
Main dimensions (in meters) of the tankers

Ship	Source	Condition	C_B	L	B	T	S
VLCC-1	MARIN	Loaded	0.850	310.0	47.2	18.9	22804
VLCC-1	MARIN	Ballasted	0.827	310.0	47.2	7.6	18670
VLCC-2	IPT	Loaded	0.832	320.0	54.5	21.6	27508
P. P. MORAES	IPT	Loaded	0.821	231.1	26.0	12.8	10304
P. P. MORAES	IPT	Ballasted	0.771	231.1	26.0	5.1	6424

parameter when $A(a) > 0$. Notice, in particular, that in this Taylor's series expansion method no stable equilibrium configuration would exist in the vicinity of the bifurcation point when $a_{CR} - a > 0$ and $A(a) < 0$.

Besides this qualitative change of behavior in the bifurcation phenomenon, it should be stressed that the term $B(a)$ depends essentially on the cross-flow coefficient C_Y (see Eq. (12b)), a hydrodynamic parameter that is certainly very robust from an experimental point of view. This result should be contrasted with the standard Taylor's series expansion method, where the post-critical behavior depends on the third order hydrodynamic derivatives $A(a)$, the confidence in the experimental determination of this term being relatively weak. Even experiments specially designed to obtain such higher order hydrodynamic derivatives show, sometimes, a wide discrepancy of results; in particular, as described in Kijima[16], different laboratories, working with models of the same ship, predict values for the hydrodynamic derivative N_{vvv}, directly related to the coefficient $A(a)$, that differ not only in magnitude but also in sign.

4. Experimental results

This section presents experimental results obtained at IPT's test basin for both the force coefficients $\{C_{1C}(\alpha); C_{2C}(\alpha); C_{6C}(\alpha)\}$ and the bifurcation and post-critical behavior of a ship exposed to a current and free to rotate around an articulation placed along the ship's axis. The force coefficients were determined by a standard captive model test while the bifurcation feature has been obtained by towing the ship by a vertical bar passing through the articulation.

The wave tank at IPT is 220 m long, 6.75 m wide and 4.50 m deep and two models have been analyzed: one for a very large tanker, named here VLCC-2 (scale 1/90), the other for the ship P. P. MORAES (scale 1/65), which has a somewhat unusually large L/B ratio for a tanker; for the sake of comparison, the force coefficients obtained at MARIN for the ship VLCC-1 (scale 1/82.5)[11] are also shown here.

In the following, the experimental results are presented and compared with the theoretical expressions derived at Sections 2 and 3 of this work.

Table 2
Experimental values $\{(C_Y)_{EXP}; (l/L)_{EXP}\}$ and Hoerner's values $(C_D)_{HOER}$

Ship	$B/2T$	$(C_D)_{HOER}$	$(C_Y)_{EXP}$	$(l/L)_{EXP}$
VLCC-1	1.25	0.84	0.60	3.0%
VLCC-1	3.11	0.60	0.50	4.8%
VLCC-2	1.26	0.85	0.84	5.9%
P. P. MORAES	1.02	0.90	1.00	1.4%
P. P. MORAES	2.55	0.60	0.50	8.6%

4.1. Force coefficients

Table 1 describes the main dimensions of the tankers that will be analyzed in this section; here the 'ballasted' condition is defined at 40% of the 'loaded' draft.

The force coefficients (Eqs. (7) and (9)) depend on the cross-flow drag coefficient C_Y and on the distance l behind the midsection where this drag force is applied. As discussed in Section 2, the cross-flow drag coefficient C_Y can be estimated by the Hoerner's curve shown in Fig. 1, while l/L should be of order 5%. Table 2 shows the measured values of C_Y and l/L together with the value of C_D from Hoerner's curve. The agreement is in general reasonable with exception of the VLCC-1 tanker in the 'loaded' condition. In particular, the difference between the experimental values of C_Y for the tankers VLCC-1 and VLCC-2 is difficult to be understood, since they have basically the same main dimensions; the only possible explanation is that for $B/2T \approx 1.25$ the drag coefficient changes rapidly with $B/2T$ (Fig. 1), suggesting that in this range of $B/2T$ the value of C_Y may be more strongly influenced by others small differences, as the bilge radius, for example.

To check the heuristic Eqs. (5), (7) and (9) one has feed them with the experimental Reynolds number 2.5×10^5 and with the values $\{(C_Y)_{EXP}; (l/L)_{EXP}\}$, since the intention was to verify the structure of the formulas in their dependence on the main dimensions and on the incidence angle α.

Fig. 3 shows the comparison between the experimental results and the heuristic expressions for the tanker VLCC-2. The agreement is reasonably good for the lateral force coefficient $C_{2C}(\alpha)$ and the yaw coefficient $C_{6C}(\alpha)$, although Eq. (7) predicts, due to the term proportional to $|\cos\alpha|$, that the maximum lateral force is not exactly at $\alpha = 90°$ but in the vicinity of this angle; some experimental support of this result can be found in Obokata *et al.*[9]. For the longitudinal force coefficient $C_{1C}(\alpha)$ both the theoretical and experimental results show the same trend, although the scatter of the experimental data is quite evident; this

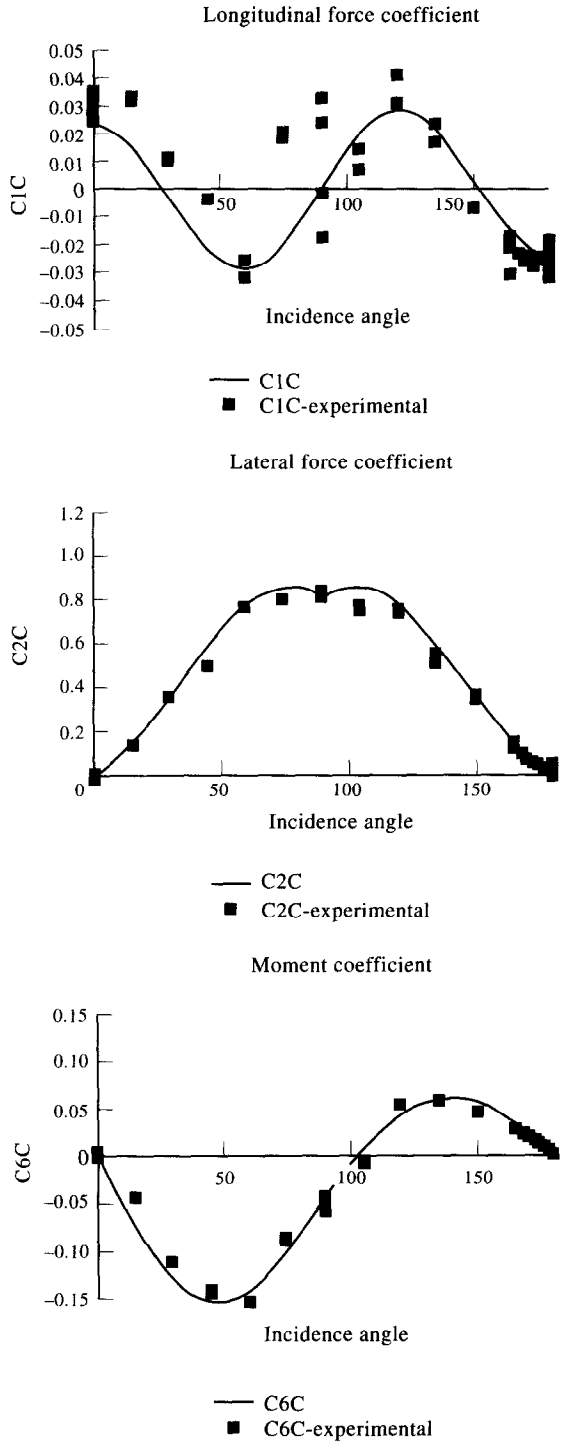

Fig. 3. Force coefficients (5), (7), (9) and experimental results for VLCC-2 ('loaded').

scatter is caused by the difficulties to measure such small values of the force.

Fig. 4(a,b) presents the same data for the tanker P. P. MORAES in the 'loaded' and 'ballasted' conditions; the overall behavior is the same as the one commented above, although the fitting between the results for the yaw coefficient is a little worse than for the VLCC-2 case, mainly in the 'ballasted' condition, where the magnitude of the moment is small. It is interesting to observe that the longitudinal force coefficient has a completely different a-dependence in the 'loaded' and 'ballasted' conditions, a difference that is captured by Eq. (5).

Table 3
Experimental and theoretical (see Eq. (11)) values of a_{CR}

Ship	Condition	$(a_{CR})_{EXP}$	$(a_{CR})_{THEO}$	Error
VLCC-2	Loaded	0.39	0.36	−7.7%
P. P. MORAES	Loaded	0.42	0.38	−9.5%
P. P. MORAES	Ballasted	0.20	0.21	5.0%

In Fig. 5(a,b) the results for the VLCC-1 are displayed, showing a similar behavior as the ones discussed in the two others cases. The only point that deserves attention here is that the source of these data is different from the other two, which enhance the confidence in the proposed expressions (in reality, the more recent OCIMF data were used instead of Wichers[11] results).

Finally, Eqs. (5), (7) and (9) could obviously be adjusted to better the fitting with the experimental results. In doing so, however, the physical meaning of the different terms could be lost and, even more, in adjusting the expressions some important terms could be missed, leading eventually to conclusions about the qualitative dynamic behavior that may not be strictly correct.

4.2. Bifurcation of the equilibrium and post-critical behavior

Consider now that the ship is being towed in a given direction by a vertical bar passing through an articulation (turret) placed at the distance aL from the midsection, with $0 < a < 0.5$ (see Fig. 2). It has been verified experimentally that for a large enough the ship's longitudinal axis is aligned with the pulling direction ($\Psi_e = 0$). As a decreases the same configuration is observed until a critical value of a, denoted by a_{CR}, is reached; for $a < a_{CR}$ the observed equilibrium configuration is such that $|\Psi_e| \neq 0$, the equilibrium angles appearing in pairs, with $\{\Psi_e \cong |\Psi_e|; \Psi_e \cong -|\Psi_e|\}$.

The region in the a-axis where the critical value is located can be easily detected from the experimental values but it is certainly difficult to exactly determine from the experiments the actual value of a_{CR}. The following procedure can be used to estimate the experimental value of this critical parameter: assuming that the articulation is approaching the midsection, let a_1 be the first point in the experiment where one observes $\Psi_e = \Psi_{e,1} \neq 0$ and $a_2 < a_1$ be the second one, with $\Psi_e = \Psi_{e,2} > \Psi_{e,1}$. Since the theory indicates (and the experimental data visually confirmed) that for small values of $a_{CR} - a$ the angle Ψ_e increases linearly with this parameter, one can estimate the position of a_{CR} by drawing a straight line between these two experimental

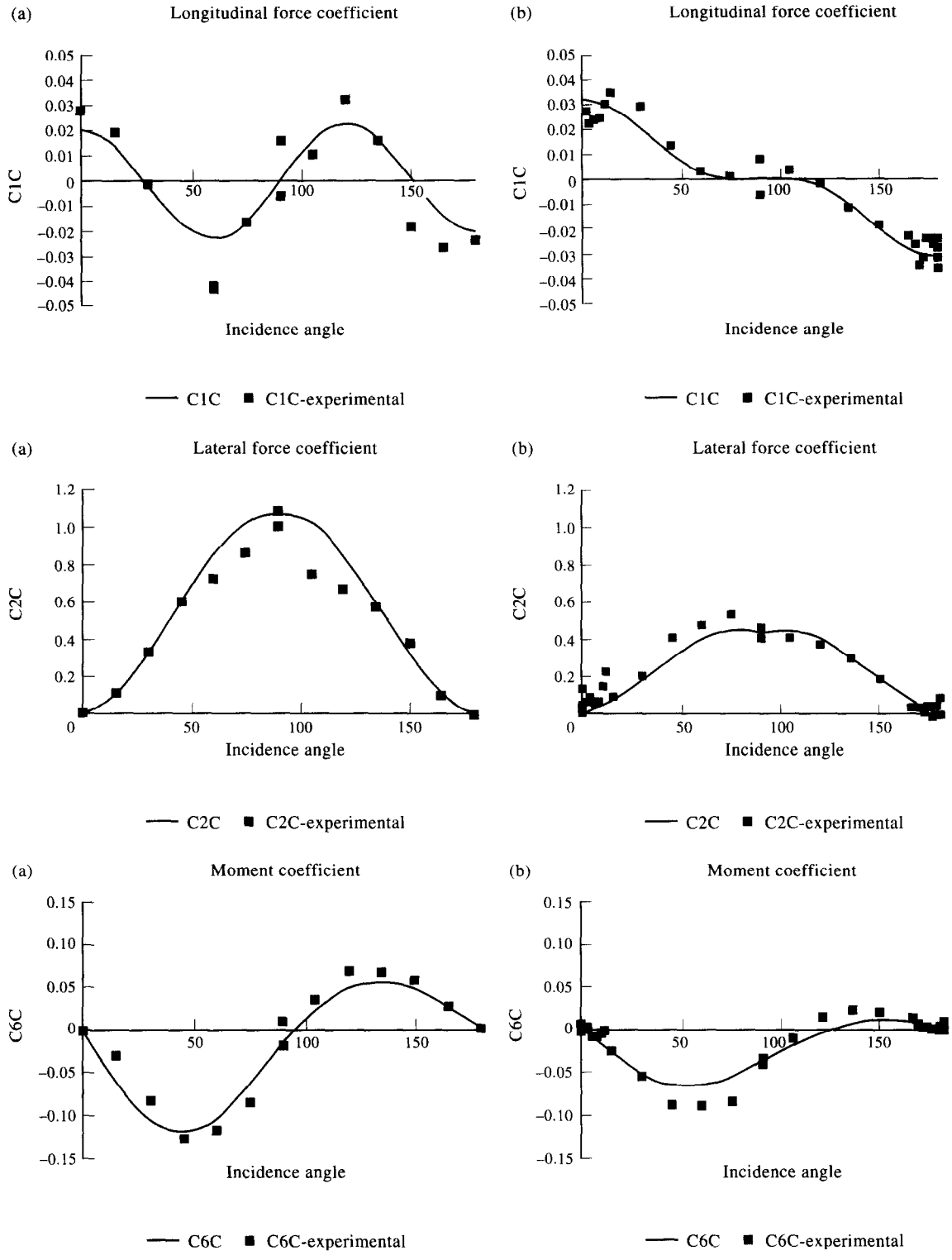

Fig. 4. (a) Force coefficients (5), (7), (9) and experimental results for P. P. MORAES ('loaded'); (b) force coefficients (5), (7), (9) and experimental results for P. P. MORAES ('ballasted').

points. This procedure was followed for the P. P. MORAES model, both in the 'loaded' and 'ballasted' condition, but for the VLCC-2 model a more visual approach was taken.

The confrontation between the theoretical prediction of a_{CR}, given by Eq. (11), and the experimental values is shown in Table 3. It turns out that Eq. (11), obtained from the *linear* hydrodynamic derivatives proposed by Clarke *et al.*[15], predicts the critical turret position with reasonable accuracy. Obviously, the theoretical result could eventually be bettered if the statistical analysis pursued by Clarke *et al.*

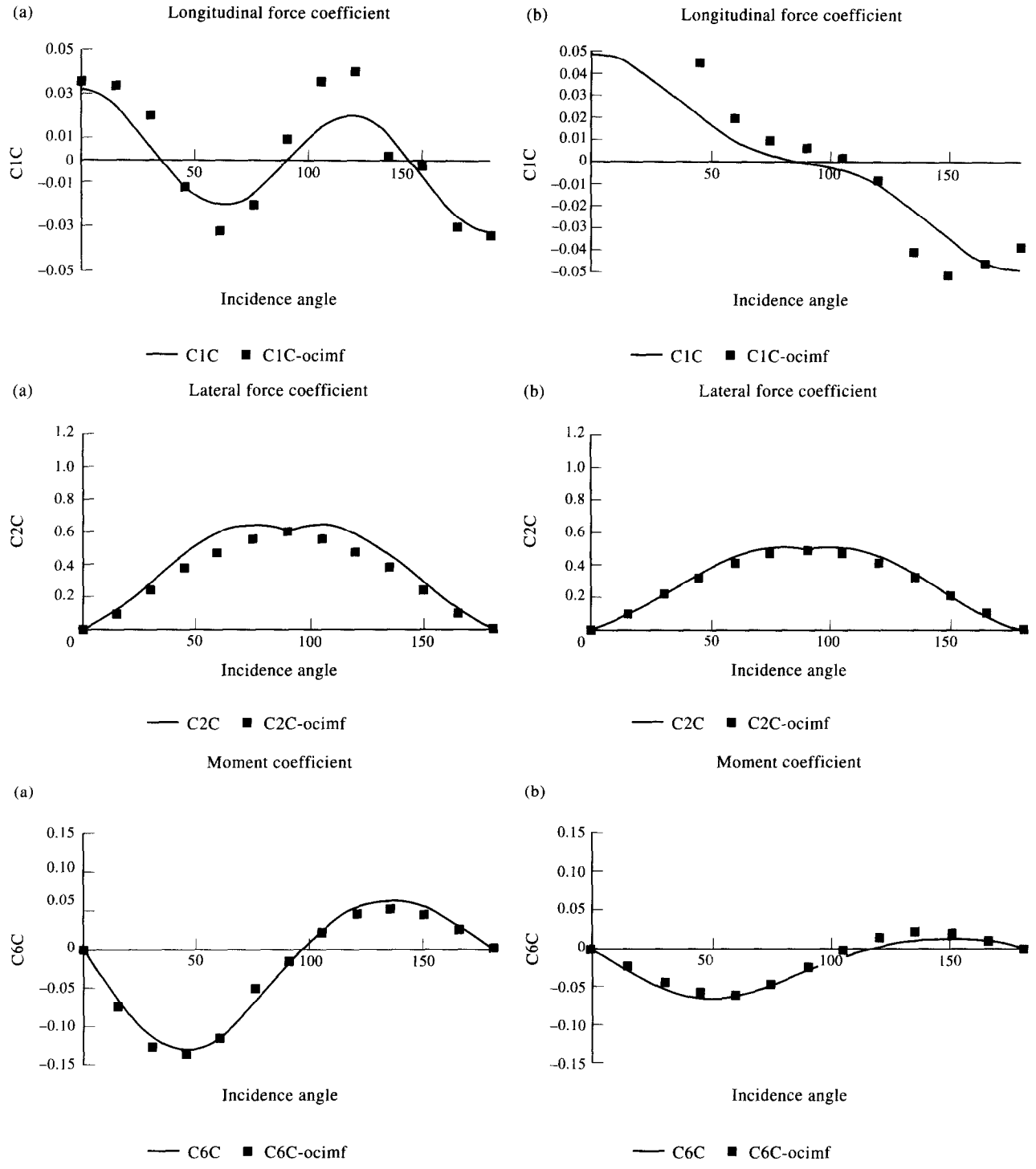

Fig. 5. (a) Force coefficients (5), (7), (9) and experimental results for VLCC-1 ('loaded'); (b) force coefficients (5), (7), (9) and experimental results for VLCC-1 ('ballasted').

were restricted to data from large tankers but this point will not be addressed here.

Assuming, in the following, $a_{CR} = (a_{CR})_{EXP}$, one can use Eq. (12b), Eq. (15a), Eq. (15b) and Eq. (15c) to determine $\Psi_e(a)$, namely, the *stable* equilibrium configuration as a function of the turret position aL; the final result has been plotted in Figs 5–7 together with the experimental values. Notice that the intention here was not to check the critical value but only the post-critical behavior, particularly the importance of the term $B(a)|\Psi_e|$ in the equilibrium Eq. (14a).

Although the theory predicts that the bifurcation phenomenon is independent of the pulling velocity, the experiments at IPT's wave tank were conducted at different velocities, aiming to assert the repeatability of the results and to verify

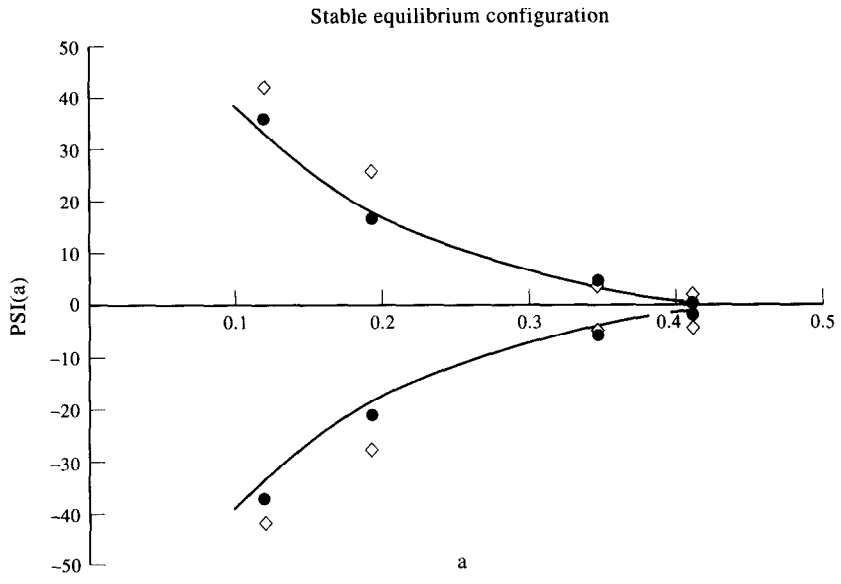

Fig. 6. Stable equilibrium configuration $\Psi_e(a)$. Case: P. P. MORAES, 'loaded'; theory: ————; experiment: $\bullet U/\sqrt{gB} = 0.10$; $\diamond U/\sqrt{gB} = 0.25$.

the sensibility of the model to 'imperfections', namely, to the possible importance of non-modeled effects, as the Froude number influence (wave generation), for example. For this reason, Figs 6–8 present the experimental values measured at two different velocities, corresponding to the *sectional* Froude number $\{U/\sqrt{gB} = 0.10; U/\sqrt{gB} = 0.25\}$ for the P. P. MORAES case and $\{U/\sqrt{gB} = 0.08; U/\sqrt{gB} = 0.24\}$ for the VLCC-2.

In the 'loaded' situation, where the current forces are large and the response should be less susceptible to 'imperfections', the measured values of $\Psi_e(a)$ at the two velocities were relatively close, although the values related to the greatest Froude number were consistently larger than the ones related to the smallest Froude number. This result indicates that some 'wave generation' effect is in fact present and influencing the experimental values, a conclusion reinforced by the analysis of the ship P. P. MORAES in the 'ballasted' condition, where the current forces are now small and the difference between the two Froude numbers results is large.

Restricting the attention to the lowest Froude number, where the wave generation effect is minimized, the agreement between the experimental results and theory is certainly consistent.

5. Conclusion

In this paper the force coefficients in a tanker, caused by an ocean current, were derived by means of a heuristic hydrodynamic model and have been checked against experimental

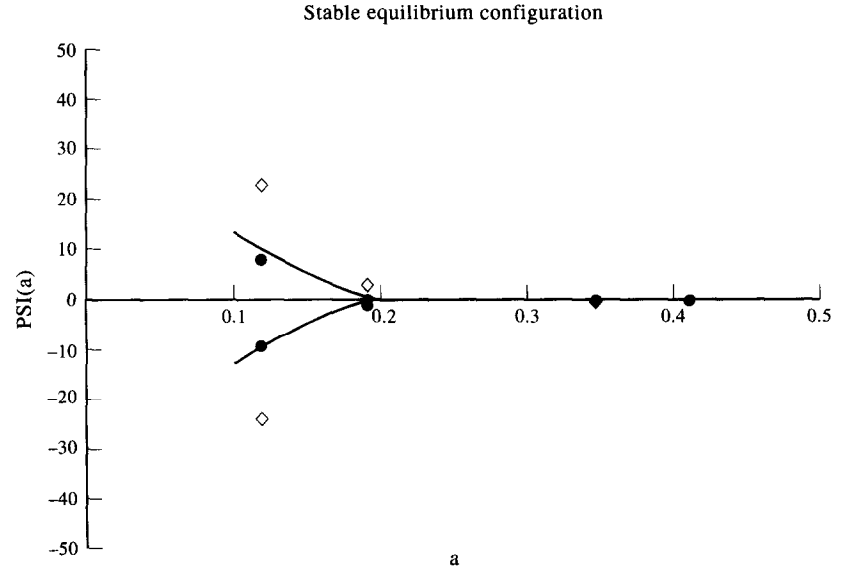

Fig. 7. Stable equilibrium configuration $\Psi_e(a)$. Case: P. P. MORAES, 'ballasted'; theory: ————; experiment: $\bullet U/\sqrt{gB} = 0.10$; $\diamond U/\sqrt{gB} = 0.25$.

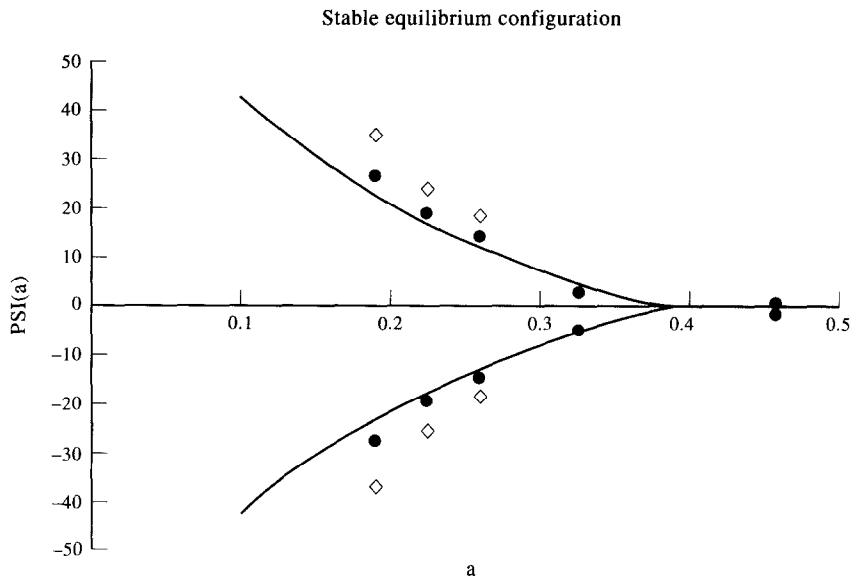

Fig. 8. Stable equilibrium configuration $\Psi_e(a)$. Case: VLCC-2, 'loaded'; theory: ————; experiment: $\bullet U/\sqrt{gB} = 0.08$; $\diamond U/\sqrt{gB} = 0.24$.

results, the adherence being reasonably good for all three force coefficients in the horizontal plane. The arguments employed to obtain these coefficients are relatively standard in ship hydrodynamics and they have been used before by several researches[9,17]; the novelty here (if any) is just to make a heuristic blend between the cross-flow expressions, valid when $|\sin\alpha| \cong O(1)$, and the expressions from the low aspect ratio wing theory, valid when $\alpha \ll 1$, incorporating in these last ones the linear maneuvering coefficients proposed by Clarke *et al.*[15].

The obtained formulas for the force coefficients were then used to predict the bifurcation and post-critical behavior of a tanker, assuming that only one degree of freedom, the yaw motion, was allowed. The observed adherence between the predicted and experimentally determined post-critical behavior was very consistent, indicating that the near critical response is dominated by the term $C_Y\Psi|\Psi|$, related to the cross-flow phenomenon. It turns out, then, that the equilibrium angle increases linearly with the bifurcation parameter, and not with its square root, as the standard Taylor's series expansion approach (hydrodynamic derivatives) indicates. Although most researches apparently prefer the traditional Taylor's series expansion to analyze the maneuvering and the stability of ships, it is important to observe at least one exception to this trend, related to the work done by Inoue *et al.*,[18] where the cross-flow term $C_Y\Psi|\Psi|$ is explicitly incorporated in the model.

The most important consequence of this work, however, is related with the questions about the reliability of the dynamic model. In fact, in the traditional approach the qualitative behavior of the system depends crucially on a consistent determination of the third order hydrodynamic derivatives $\{Y_{vvv}; N_{vvv}\}$, a relatively difficult task from an experimental point of view; in particular, even the sign of these coefficients are sometimes predicted in different ways depending on the source of the experimental data. In contrast, it has been shown here that the post-critical behavior depends essentially on the value of the cross-flow coefficient C_Y, a hydrodynamic parameter that can be determined with relative accuracy.

Acknowledgements

This work has been partially supported by Petrobrás. The first author also aknowledges a scholarship from Petrobrás, and the second author a scholarship from CNPq.

References

[1] Henery D, Inglis RB. Prospects and challenges for FPSO. In *Proceedings of the 27th Offshore Technology Conference*, Paper OTC-7695, 2. OTC, Houston, TX, USA, 1995, pp. 9–21.

[2] Mack RC, Gruy RH, Hall RA. Turret moorings for extreme design conditions. In *Proceedings of the 27th Offshore Technology Conference*, Paper OTC-7696, 2. OTC, Houston, TX, USA, 1995, pp. 9–21.

[3] Papoulias FA, Bernitsas MM. Autonomous oscillations, bifurcations and chaotic response of moored vessels. Journal of Ship Research 1988;32(3):220–228.

[4] Garza-Rios LO, Bernitsas MM. Analytical expressions of the stability and bifurcation boundaries for general mooring systems. Journal of Ship Research 1996;40(4):337–350.

[5] Bernitsas MM, Garza-Rios LO. Effect of mooring line arrangement on the dynamics of spread mooring systems. Journal of Offshore Mechanics and Artict Engineering 1996;188(1):7–20.

[6] Nishimoto K, Brinati H, Fucatu C. Dynamics of moored tankers, SPM and turrets. In *Proceedings of the 6th International Offshore and Polar Engineering Conference*, ISOPE, 26–31 May 1996. ISOPE, Los Angeles, CA, USA, 1996.

[7] Fernandes AC, Aratanha M. Classical assessment to the single point mooring and turret dynamic stability problems. In *Proceedings of the International Conference of Offshore Mechanics and Artict Engineering*. OMAE, Florence, Italy, 1996.

[8] Pesce CP, Tanuri EA. Stability and dynamics of offshore single point mooring systems. *Revista Brasileira de Ciências Mecânicas* (to appear).

[9] Obokata J, Sasaki N, Nakajima J. On the estimation of current force induced on a ship hull by some model tests (in Japanese). Association of the Naval Architects of Western Japan 1981;180:47–57.

[10] Takashina J. Ship manoeuvering motion due to tugboats and its mathematical model. Journal of the Society of Naval Architects of Japan 1986;160:93–104.

[11] Wichers JEW. *A Simulation Model for a Single Point Moored Tanker*. Publ. 797, MARIN, Wageningen, the Netherlands, 1988 (see also *Prediction of Wind and Current Loads on VLCCs*, OCIMF Report No. 211524-2-OE, OCIMF, 1993).

[12] Van Manem JD, Van Oossanen P. Resistance. In *Principles of Naval Architecture*, Vol. 2, Ch. 5, 2nd Rev. Society of Naval Architects and Marine Engineers, 1988.

[13] Hoerner SF. Fluid Dynamic Drag, authors publication, New Jersey, USA, 1965.

[14] Taylor GI. Analysis of the swimming of long and narrow animals. Proceedings of Royal Society A 1952;214:158–183.

[15] Clarke D, Gedling P, Hine G. The application of manoeuvring criteria in hull design using linear theory. In *Proceedings of the Royal Institute of Naval Architects*. Royal Institute of Naval Architects, 1983, pp. 45–68.

[16] Kijima K. Influence of model scale in the determination of the hydrodynamic derivatives (in Japanese). Bulletin of the Society of Naval Architects of Japan 1996;801/3:25–30.

[17] Faltinsen OM. *Sea Loads on Ships and Offshore Structures*. Cambridge University Press, 1990.

[18] Inoue S, Hirano M, Kijima K. Hydrodynamic derivatives on ship maneuvering. International Ship Building Progress 1981;28(321): 112–125.